SUPPORTING MATERIAL

"A physical model reveals the mechanochemistry responsible for dynein's processive motion"

D. Tsygankov, A.W.R. Serohijos, N.V. Dokholyan, and T.C. Elston

A. Shape and flexibility of dynein motor domains

The EM-images from Burgess *et al*.[1] suggest the shape of a single dynein head can be described by three subunits that move relative to each other: 1) the AAA+ ring, which is represented as a circle of fixed radius ($R = 6.7$ nm), 2) the stalk, described as a flexible circular arc of a fixed length, $L_s = 13.9$ nm, which emerges perpendicularly from the AAA+ ring and 3) the tail, described as a flexible circular arc of a fixed length, $L_t = 26.0$ nm, which immerges tangentially from the AAA+ ring. The linker connecting the tail and the ring presumably lies across the ring and is only visible when the molecule assumes special "undocked" conformations[1]. In this work we do not consider linker undocking events.

At each instance of time, the shape of a dynein head is described by three angles, $X = \{\alpha, \beta, \gamma\}$. The angle $\alpha \in [-\pi, \pi]$ determines the curvature of the stalk, the angle $\beta \in [-\pi, \pi]$ determines the curvature of the tail, and the angle, γ, determines the arc length between the points where the stalk and the tail emerge from the ring (Fig. 1 in the main text and Fig. S1A). We used the images of Burgess and coworkers[1] to compute distributions for these angles in the pre-stroke and post-stroke conformations. These distributions have a characteristic bell-shape (e.g. Fig.3g in Ref. [1]) and provide an estimate for the mean and variance of each angle. Our estimations for the mean values, μ_X, and standard deviations, σ_X for each angle in both pre- and post- power stroke conformations are given in Table S1.

Table S1: Geometric parameters of dynein heads.

	μ_α	$3\sigma_\alpha$	μ_β	$3\sigma_\beta$	μ_γ
pre-stroke	49.7925°	38°	15.5173°	44°	86.0°
post-stroke	8.7818°	34°	32.0585°	44°	28.5°

We use the estimated distributions to define an energy function E_S

$$E_S = -k_B T \sum_X \log(\rho_X), \tag{1}$$

where

$$\rho_X = \exp\left(-\frac{(X-\mu_X)^2}{2\sigma_X^2}\right). \tag{2}$$

Using this function to investigate the bending energy of dynein dimers interacting with a microtubule, we discovered that the configuration in which the two heads are 8.2 nm apart with the leading head in the pre-stroke conformation and the rear head in the post-stroke conformation represents the minimum energy state. That is, in this configuration both heads adopt their mean (zero energy) conformation. This analysis suggests that dynein's structure evolved to form a dimer with the microtubule binding domains (MTBDs) of the heads separated by a distance equal to the microtubule period.

Because each dynein head has two flexible protrusions (the stalk and tail), it is natural to expect that under thermal fluctuations two-headed dynein would show a very wide range of motion. Fig. 1 in the main text demonstrates the $3\sigma_\alpha$ range of motion for the stalk and $3\sigma_\beta$ range of motion for the tail with the position of the AAA+ ring fixed. Similar results are shown in Fig. S1B,C, but with the position of the MTBD fixed to represent the case in which the stalk is tightly bound to the microtubule. In this case, the ring and the tip of the tail swing over a range of ~20 nm and ~30 nm, respectively. Remarkably, when the tail of an unbound head is tightly attached to the tail of the bound head, the range of motion of the unbound MTBD is greatly restricted (Fig. 2). The constraints imposed by the structure of dynein allow the unbound MTBD to quickly approach the appropriate binding site (Fig. 2). Once again we see that dynein structure is tuned to make it a highly efficient motor (see also Fig. S2B,C).

Although the full scale structure of the motor domains is extracted from the EM images of *axonemal* dynein[1], we use estimates of biochemical rates from experimental data on both axonemal and cytoplasmic isoforms. Using our low-dimensional representation of the heads, we assume it to be valid for both types of dyneins. Because we are interested in studying the mechanism of processive stepping we compare step-size distributions from our simulations with single-molecule experiments on the *cytoplasmic* motor[2].

B. Dynein stepping

Starting from the configuration in which both heads are bound to the microtubule, each head-over-head step of the motor involves detachment of the trailing head, biased diffusion of this head to a binding site in front of the bound head and reattachment, so that the initial and the final states of the dimer are mechanically identical except with the relative position of the heads reversed (Fig. 1E). According to our previous analysis[3], two-headed dynein binds to microtubule with the leading and trailing heads in the pre- and post-stroke conformations, respectively. Thus, each dynein step includes two transitions: a power-stroke (transition of the leading head from a pre- to post-stroke conformation) and recovery (transition of the trailing head from a post- to pre-stroke conformation). The nature of these transitions is stochastic (Supplementary Movie S2). However, to illustrate the dominant motion of the heads during the stepping cycle, we first consider a situation in which the geometry of the two heads transitions deterministically at a constant rate between their pre- and post- stroke conformations. That is, we change the parameters $X = \{\alpha, \beta, \gamma\}$ in small increments from their pre- to post-stroke values for the front head and vice versa for the rear head. A surprising property for the motion of the rear head emerges. The MTBD of this head moves along a straight line from its starting point at a rear binding site to a new binding site in front of the other head (Fig. S3A). Thus the MTBD slides over microtubule surface and reaches next binding site along the shortest possible path (Supplementary Movie S1).

Given the flexibility of the motor and the large effects of thermal fluctuations, we cannot expect dynein to move exactly along the deterministic path shown above. However, our observation explains the tendency of the unbound MTBD to stay close to the microtubule during the diffusion process. Other conclusions from this analysis are:

1. The point where the tails are linked moves parallel to the microtubule during the step. As we demonstrated before, the tip of the tail is the most mobile part of the attached head (Fig. S1B,C). In the cytoplasm, the tail tip is free to fluctuate over a significant distance. However, in

the axoneme, dyneins step along a microtubule doublet with their tails permanently attached to an adjacent parallel microtubule doublet[4-6]. Thus, dyneins structure seems to be tuned to step efficiently in the conditions of the axoneme, where the motion of the tails is constrained.

2. Dynein's AAA+ rings have to shift sufficiently with respect to each other to allow the MTBD of the free head to cover the 16.4 nm between binding sites. However, as can be easily seen in Supplementary Movie S1, the motion of the rings during the step includes both a shift and rotation. This motion proceeds in such a way that there is a point on each ring that remains in apposition throughout the step. That is, if we move the reference frame so that the origin coincides with the point on the ring located 5.60 nm from the ring center and 53.7° from the point where the stalk emerges, the relative motion of the rings appears as a pure rotation around the origin. This reference frame translates horizontally with respect to the microtubule as the motor steps. The existence of such a pivot point is not trivial, but a unique outcome of the geometry of the heads and relative movement of their subunits[1] (see "back-stepping" section below for comparison).

One important implication of this point is that it represents a good candidate for a site of physical interaction between the rings[3]. A bond at this point would not interfere with the heads motion during stepping, and in fact likely may reduce deviations in the motor's step size.

3. A number of models for dynein's power-stroke have been suggested[1, 7-9]. A shortcoming of these models is that they focus on a single head. The role of the power-stroke of the bound head is to bias the motion of the free head towards a forward binding site. Thus, any realistic model of the power-stroke must take into consideration both heads. Moreover, our stepping model reveals that the recovery of the free head is equally important in biasing the free head toward a forward binding site. The overall effect of the power-stroke and the recovery is the translocation of the MTBD of the free head in the forward direction parallel to the microtubule: the most logical and straightforward mechanism for a two-headed motor. Note that to understand the stepping mechanism it is important to consider the full motion of the bound head during the power stroke, not only the relative position of the tail and the stalk (Fig. S1D).

4. Finally, the deterministic analysis allows us to understand how the order of the power-stroke and recovery of the bound and free heads affects forward stepping. The analysis above considered these two transitions to occur simultaneously, but what happens if the power-stroke precedes the recovery or vice versa? As demonstrated in Fig. S3B, the movement of the free MTBD during the power-stroke of the bound head (red) while the free head (blue) remains in post-stroke conformation. At the end of the transition the heads overlap in the post-stroke conformation (green), but during the power-stroke the trajectory of the free MTBD (blue curve) lies above the microtubule with the initial motion (black arrow) directed up and forward. In contrast, if the recovery of the free head occurs before the power stroke, the initial motion is pointed downward with the trajectory of the MTBD lying below the microtubule surface (Fig. S3C). In this case, the microtubule will interfere with the motion of the MTBD, so that the bound head will have to deform or pivot forward to allow the free head to move in a forward direction. As demonstrated in our full simulations, the net result of this motor-microtubule interaction is that the probability of taking a back-step is higher when the recovery of the free head precedes the power-stroke of the bound head (Fig. 3B).

Back-stepping

A similar deterministic approach can be used to understand processive back-stepping. When the free head in pre-stroke conformation attaches behind (rather than in front of) the bound head after completion of the power-stroke, the motor assumes a high energy conformation as shown in Fig. 4D in the main text. Until the motor recovers back to the low energy conformation, subsequent power-stroke and recovery transitions lead to the backward stepping as demonstrated in Movie S3. In this case, the motion of AAA+ rings consists mostly of a parallel shift with very little rotation. In contrast to forward stepping, such motion disrupts the compact conformation and no inter-ring contact can be retained during the stepping cycle.

C. Dynein stepping simulation

To simulate dynein's processive stepping we constructed a hybrid routine where Structural Dynamics (SD) of the motor is incorporated into Monte Carlo (MC) simulations of its mechanochemical cycle.

1. Structural dynamics simulations

The full description of two headed dynein requires 6 coordinates for each head: the position of the ring center, (x_i, y_i), the rotation of the ring around its center, φ_i, and the shape parameters $(\alpha_i, \beta_i, \gamma_i)$, where *i* = 1,2 and indexes the heads (Fig. S2A). These coordinates define the angle between the tail tips, ξ, and the angles between the stalk tip and the microtubule, δ_i (see Fig. S2A).

To simulate the bond between the tails, described by the angle ξ, and the MTBD and microtubule bonds, described by the angles δ_i, we add the following terms to the energy function, E_S, given by Eq. (1):

$$E = E_S + k_B T\left[\frac{r_t^2}{2\sigma_t^2} + \frac{\left(\xi - \mu_\xi\right)^2}{2\sigma_\xi^2} + \sum_{i=1,2} C_i\left\{\frac{r_i^2}{2\sigma_s^2} + \frac{\left(\delta_i - \mu_\delta\right)^2}{2\sigma_\delta^2}\right\}\right] \tag{3}$$

where r_t is the distance between the tail tips, r_i is the distance between each MTBD and the nearest binding site on the microtubule and

$$C_i = \begin{cases} 1, & \text{if head } i \text{ is bound} \\ 0, & \text{if head } i \text{ is unbound} \end{cases} \tag{4}$$

Here, parameters μ_ξ and μ_δ correspond to a preferred angle for the bonds between the tails and MTBD and microtubule, respectively. In our simulations, we use $\mu_\xi = 0$ and $\mu_\delta = \pi/2$. Parameters σ_ξ and σ_δ define ranges of deviations from the preferred orientations at the bonds. We use these quantities as tuning parameters to explore the effects of bond flexibility on the stepping properties of the motor (Fig. 3A-C in the main text). Finally, σ_t and σ_s define allowed variations in the bond length, which we choose to be reasonably small (2 Å). In our simulations we consider the binding event occurred when the position and orientation of the unbound MTBD satisfied conditions $r_i < 3\sigma_s$ and $\left|\delta_i - \mu_\delta\right| < 3\sigma_\delta$.

Using the energy function *E* given by Eq. (3), we update each coordinate, $X = \{x_i, y_i, \varphi_i, \alpha_i, \beta_i, \gamma_i\}$ using the following discretization of the Langevin equations:

$$X(t+\Delta t) = X(t) - D_X \Delta t \frac{\partial U}{\partial X} + \sqrt{2 D_X \Delta t}\ N(0,1), \tag{5}$$

where D_X is the diffusion constant, $N(0,1)$ is a normally distributed random process with zero mean and unitary variance, $U = E/k_B T$ is the energy function in the units of $k_B T$. For each coordinate we need to define the value of the corresponding diffusion constant. For x_i, y_i, φ_i, α_i and β_i the diffusion constants can be estimated using the Einstein relation, Stokes' law and geometrical arguments: $D \sim \frac{k_B T}{6\pi r \eta}$, while the constant D_γ is chosen based on the expected rate of the biased diffusion as $D_\gamma \sim \frac{rate}{2}\left(\gamma_{\text{pre}} - \gamma_{\text{post}}\right)^2$. Table S2 gives the values that were used in our simulations.

Table S2: The values of diffusion coefficients used in the simulations.

$D_x\ (\text{nm}^2\text{ns}^{-1})$	$D_y\ (\text{nm}^2\text{ns}^{-1})$	$D_\varphi\ (\text{rad}^2\text{ns}^{-1})$	$D_\alpha\ (\text{rad}^2\text{ns}^{-1})$	$D_\beta\ (\text{rad}^2\text{ns}^{-1})$	$D_\gamma\ (\text{rad}^2\text{ns}^{-1})$
0.0350	0.0350	4.4e-5	1.4e-3	4.1e-4	4.1e-5

For the AAA+ ring of 13.4 nm in diameter, assuming $k_B T = 4 \cdot 10^{-21} J$ and viscosity $\eta = 0.9 \cdot 10^{-3} (Pa \cdot s)$, the diffusion coefficient is $D_x = 3.5 \cdot 10^{-11} (m^2/s)$, so that along a straight line the stepping distance of 16.4 nm would be covered in $\tau_1 = (16.4 \cdot 10^{-9})^2 / (2 \cdot 3.5 \cdot 10^{-11}) \approx 4\,\mu s$. In case of a free diffusion in two dimensions, the mean time to approach a binding site with a capture distance 0.4 nm can be roughly estimated as $\tau_2 = 2\pi\tau_1/(0.4/16.4) \approx 1\,ms$. Taking into account the need for a proper head orientation before the binding event, the search time of a binding site would be even longer. However, our structural dynamics simulations show that for reasonably fast rates of the power-stroke and recovery, the biased diffusion takes time of the order of τ_1, rather than τ_2, so that the free head motion is constrained by the overall motor structure to a near one-dimensional sliding.

2. Simulation of power-stroke and recovery

To simulate pre- to post- power stroke and post- to pre- power stroke transitions we use a double-well potential, which we build with three smoothly linked parabolas. The local minima E_{post} and E_{pre} are located at $\gamma_{\text{post}} = 28.5^\circ$ and $\gamma_{\text{pre}} = 86.0^\circ$, and a local maximum (barrier) E_{bar} located at $\gamma_{\text{bar}} \in (\gamma_{\text{post}}, \gamma_{\text{pre}})$. The energy profile E_γ is described by the following formula:

$$E_\gamma = \begin{cases} E_{\text{post}} + 0.5\,a\left(\gamma - \gamma_{\text{post}}\right)^2, & \text{for} \quad \gamma \le \gamma_1 \\ E_{\text{bar}} - 0.5\,b\left(\gamma - \gamma_{\text{bar}}\right)^2, & \text{for} \quad \gamma_1 < \gamma \le \gamma_2 \\ E_{\text{pre}} + 0.5\,a\left(\gamma - \gamma_{\text{pre}}\right)^2, & \text{for} \quad \gamma_2 < \gamma \end{cases} \tag{6}$$

where the constants are:

$$E_{\text{bar}} = E_{\text{post}} + \frac{(a+b)}{2ab}\left(\frac{ab(\gamma_{\text{pre}} - \gamma_{\text{post}})}{2(a+b)} + \frac{E_{\text{pre}} - E_{\text{post}}}{\gamma_{\text{pre}} - \gamma_{\text{post}}}\right)^2, \quad \gamma_{\text{bar}} = \frac{\gamma_{\text{pre}} + \gamma_{\text{post}}}{2} + \frac{(a+b)(E_{\text{pre}} - E_{\text{post}})}{ab(\gamma_{\text{pre}} - \gamma_{\text{post}})},$$

$$\gamma_1 = \frac{0.5b\gamma_{\text{pre}} + (a+0.5b)\gamma_{\text{post}}}{a+b} + \frac{E_{\text{pre}} - E_{\text{post}}}{a(\gamma_{\text{pre}} - \gamma_{\text{post}})}, \quad \gamma_2 = \frac{(a+0.5b)\gamma_{\text{pre}} + 0.5b\gamma_{\text{post}}}{a+b} + \frac{E_{\text{pre}} - E_{\text{post}}}{a(\gamma_{\text{pre}} - \gamma_{\text{post}})}.$$

The double-well potential if fully defined by γ_{post} and γ_{pre}, parameters a, b, and the energy difference $E_{\text{pre}} - E_{\text{post}}$.

For the pre- and post-stroke conformations we assign $E_{\text{pre}} - E_{\text{post}} = 12.5k_BT$ (Fig. S4A) and $E_{\text{pre}} - E_{\text{post}} = -12.5k_BT$ (Fig. S4B), respectively. This way, by switching the two forms of the potential energy as the chemical state of the head changes, we reproduce stochastic transitions corresponding to the power-stroke and recovery. The total input of energy into the system on each cycle is equal to the energy available from the ATP hydrolysis, $\Delta G = 25k_BT$. However, within a reasonable range, the exact values for the energy difference and parameters a and b are less important than the value of the diffusion coefficient, D_γ, which defines the mean time of the transitions.

3. MC simulations of dynein's mechanochemical cycle

Simulation of the structural dynamics of the dynein heads is only a part of the full mechanochemical cycle. These dynamics must be properly incorporated into a sequence of biochemical steps for the heads. In our previous work, we conducted a detailed kinetic analysis for the chemical cycle that drive dynein stepping[3]. The starting point for our analysis was the general network of all possible biochemical states. By considering the experimentally measured velocity and processivity of the motor, we derived constraints for unknown kinetic rate constants and head-head coordination. The two major results from the analysis are: 1) The rate of ADP release is significantly faster when both heads are attached to the microtubule. 2) The rate of the power-stroke by the front head is significantly faster when the rear head is detached.

Each head goes through a cycle of biochemical states: ATP binding and head detachment, recovery, hydrolysis, phosphate release and head attachment, power-stroke, and ADP release[10, 11]. The states of each head are $i = \{T^*, T, DP, D, D^*, \varnothing^*\}$, where T, D, P stands ATP, ADP, and inorganic phosphate, respectively, $\varnothing$ represents a nucleotide free head, and the asterisk indicates states in a post-stroke conformation. Suppose at time t one head is in a state i while the other head is in a state j, so that the state of the dimer is (i, j). There are two possible transitions (direction) from this state: one to $(i+1, j)$ and the other to $(i, j+1)$ (Fig. S4C).

We use the following algorithm to perform the full simulations. For transitions that correspond to a biochemical process (ATP binding, hydrolysis, Pi release, or ADP release), we simulate transition time as

$$\tau = \frac{-\log(rand)}{u_{i\to i+1}^{j\to j} + u_{i\to i}^{j\to j+1}}, \tag{8}$$

where $u_{i\to i+1}^{j\to j}$ and $u_{i\to i}^{j\to j+1}$ are the transition rates and $rand$ is a random number uniformly distributed between 0 and 1. We next determine which transition occurred based on the probabilities:

$$p_{i\to i+1}^{j\to j}=\frac{u_{i\to i+1}^{j\to j}}{u_{i\to i+1}^{j\to j}+u_{i\to i}^{j\to j+1}} \quad \text{and} \quad p_{i\to i}^{j\to j+1}=\frac{u_{i\to i}^{j\to j+1}}{u_{i\to i+1}^{j\to j}+u_{i\to i}^{j\to j+1}} \tag{7}$$

During this time (from t to $t+\tau$) we perform SD simulations of the motor dynamics under the fixed mechanical conditions: a bound head stays bound, a free head stays free, and the conformational states remain unchanged.

In contrast, for transitions that involve mechanical motion (power-stroke, recovery, or attachment), we run SD simulations until the processes is completed (e.g. the conformation of the head changes or the MTBD attaches to a binding site). In this case, the transition time τ is determined by the dynamic simulations. This way the stochastic motion of the dynein heads is simulated throughout the full mechanochemical cycle with all biochemical processes taken into account.

References

1. Burgess, S.A., Walker, M.L., Sakakibara, H., Knight, P.J. & Oiwa, K. Dynein structure and power stroke. *Nature* **421**, 715-718 (2003).
2. Reck-Peterson, S.L. *et al.* Single-molecule analysis of dynein processivity and stepping behavior. *Cell* **126**, 335-348 (2006).
3. Tsygankov, D., Serohijos, A.W., Dokholyan, N.V. & Elston, T.C. Kinetic models for the coordinated stepping of cytoplasmic dynein. *J Chem Phys* **130**, 025101 (2009).
4. Satir, P. & Christensen, S.T. Overview of structure and function of mammalian cilia. *Annu Rev Physiol* **69**, 377-400 (2007).
5. Nicastro, D., McIntosh, J.R. & Baumeister, W. 3D structure of eukaryotic flagella in a quiescent state revealed by cryo-electron tomography. *Proc Natl Acad Sci U S A* **102**, 15889-15894 (2005).
6. Nicastro, D. *et al.* The molecular architecture of axonemes revealed by cryoelectron tomography. *Science* **313**, 944-948 (2006).
7. Mizuno, N., Narita, A., Kon, T., Sutoh, K. & Kikkawa, M. Three-dimensional structure of cytoplasmic dynein bound to microtubules. *Proc Natl Acad Sci U S A* **104**, 20832-20837 (2007).
8. Carter, A.P. *et al.* Structure and functional role of dynein's microtubule-binding domain. *Science* **322**, 1691-1695 (2008).
9. Ueno, H., Yasunaga, T., Shingyoji, C. & Hirose, K. Dynein pulls microtubules without rotating its stalk. *Proc Natl Acad Sci U S A* **105**, 19702-19707 (2008).
10. Mogami, T., Kon, T., Ito, K. & Sutoh, K. Kinetic characterization of tail swing steps in the ATPase cycle of Dictyostelium cytoplasmic dynein. *J Biol Chem* **282**, 21639-21644 (2007).
11. Imamula, K., Kon, T., Ohkura, R. & Sutoh, K. The coordination of cyclic microtubule association/dissociation and tail swing of cytoplasmic dynein. *Proc Natl Acad Sci U S A* **104**, 16134-16139 (2007).

Figure legends:

Figure S1: A. Electron-microscopy images of dynein heads (by Burgess *et al*.[1]) fit with circles of a fixed radius and circular arcs with different curvatures. Red and blue shapes represent the heads in pre- and post- power stroke conformations, respectively. **B,C.** Three standard deviation range of motion of a dynein head tightly bound to a microtubule (not shown), so that the microtubule binding domain (MTBD) is fixed in space. **B:** post- power stroke conformation. **C:** pre-power stroke conformation. **D.** Power-stroke transition of a tightly bound head from pre-stroke (red) to post-stroke (blue) conformations. The combined effects of the linker (not shown), the tail and the stalk motion produce a displacement of the tail tip almost parallel to the microtubule (green).

Figure S2: A. Schematic of the coordinate system for two-headed dynein. $\{\alpha, \beta, \gamma\}$ define the shape and the conformation of the heads. $\{x, y, \varphi\}$ define the position and rotation of the ring centers. ξ and δ characterize relative orientation of the heads at the point of the tail junction and microtubule attachments, respectively. **B,C.** Simulated trajectory of dynein with one tightly bound and one unbound head. **B:** The rear head is bound in a post-stroke conformation, while the leading head is free in a pre-stroke conformation and doesn't interact with the microtubule (i.e. goes through it). **C:** The leading head is bound in a pre-stroke conformation, while the rear head is unbound in a post-stroke conformation and does interact with the microtubule (i.e. cannot go through). Red dots indicate the positions (at different time points) of the MTBDs. Green and blue dots are the positions of the ring centers of the bound and unbound heads, respectively. Finally, cyan dots are the positions of the tail tips. Contour lines show the distribution of points in plane.

Figure S3: A. Deterministic step: simultaneous uniform transitions of the bound head from pre-stroke (red) to post-stroke (magenta) and the unbound head from post-stroke (blue) to pre-stroke (cyan). The resulting trajectory of unbound MTBD is a straight line between initial (0 nm) and final (16.4 nm) binding sites on the microtubule. The blue and red dashed curves show the trajectories of the ring centers. The black dashed curve shows the trajectory of the tip of the tails. **B.** Trajectory of the unbound head (blue) in the fixed post-stroke confirmation during the power-stroke of the bound head. **C.** Trajectory of the unbound head (blue) during its recovery while the bound head remains in pre-stroke conformation. The final position of the head is indicated by the green color. The black arrows show the direction of MTBDs at the beginning of the transitions.

Figure S4: A,B. Double-well potential for power-stroke and recovery simulations. The potential is composed of three parabolas (red, green and blue) smoothly connected at γ_1 and γ_2. Local minima are located at the pre- and post-stroke values of γ. **A:** the shape of the potential with global minimum at post-power stroke orientation. **B:** the shape of the potential with global minimum at pre-power stroke orientation. The switch between these potentials initiates the stochastic transition from one conformational state to another. The height of the barrier is chosen small enough to allow thermal fluctuations to drive the transition. **C.** Mechanochemical state network for two headed dynein. Each ellipse indicates a pair of mechanochemical states of each head. Forward transitions are from left to right for one head and from top to bottom for the other one. States in the last row are transitioned back to corresponding states in the first row so that the cycle is looped. The same is true for the states in columns. *T** to *T* means recovery of the head with bound ATP; *T* to *DP* means hydrolysis; *DP* to *D* is phosphate

release, *D* to *D** is power-stroke, *D** to *Ø** is ADP release, *Ø** to *T** is ATP binding. A head is bound to microtubule in *D*, *D** and *Ø** states and unbound in *T**, *T*, and *DP* states. Finally, the blue states indicate the dominant pathway of a fast highly processive dynein with head-over-head stepping, as determined in our previous work[3].

Movie legends:

Movie S1: Relative motion of the two dynein heads during the *forward* stepping cycle. In this movie the heads move deterministically and undergo the power-stroke and recovery transitions in an out-of-phase manner.

Movie S2: Stochastic simulation of dynein's motion along a microtubule. Both processive forward and backward steps occur during the simulation. The subunits of the head domains are color coded: AAA+ ring (red), tail (blue) and stalk (green). The microtubule is shown in gray.

Movie S3: Relative motion of the two dynein heads during the *backward* stepping cycle In this movie the heads move deterministically and undergo the power-stroke and recovery transitions in a out-of-phase manner.

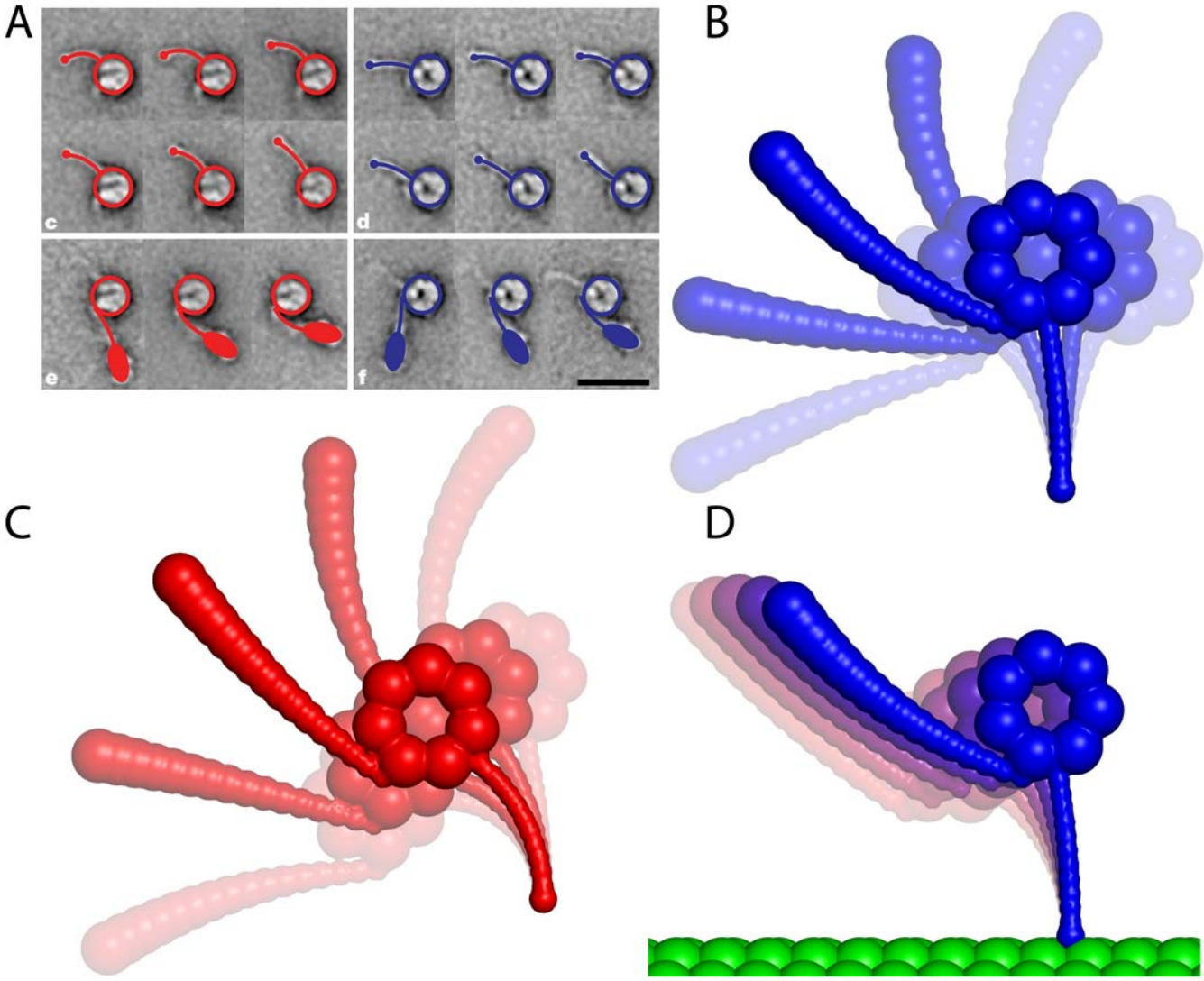

Figure S1

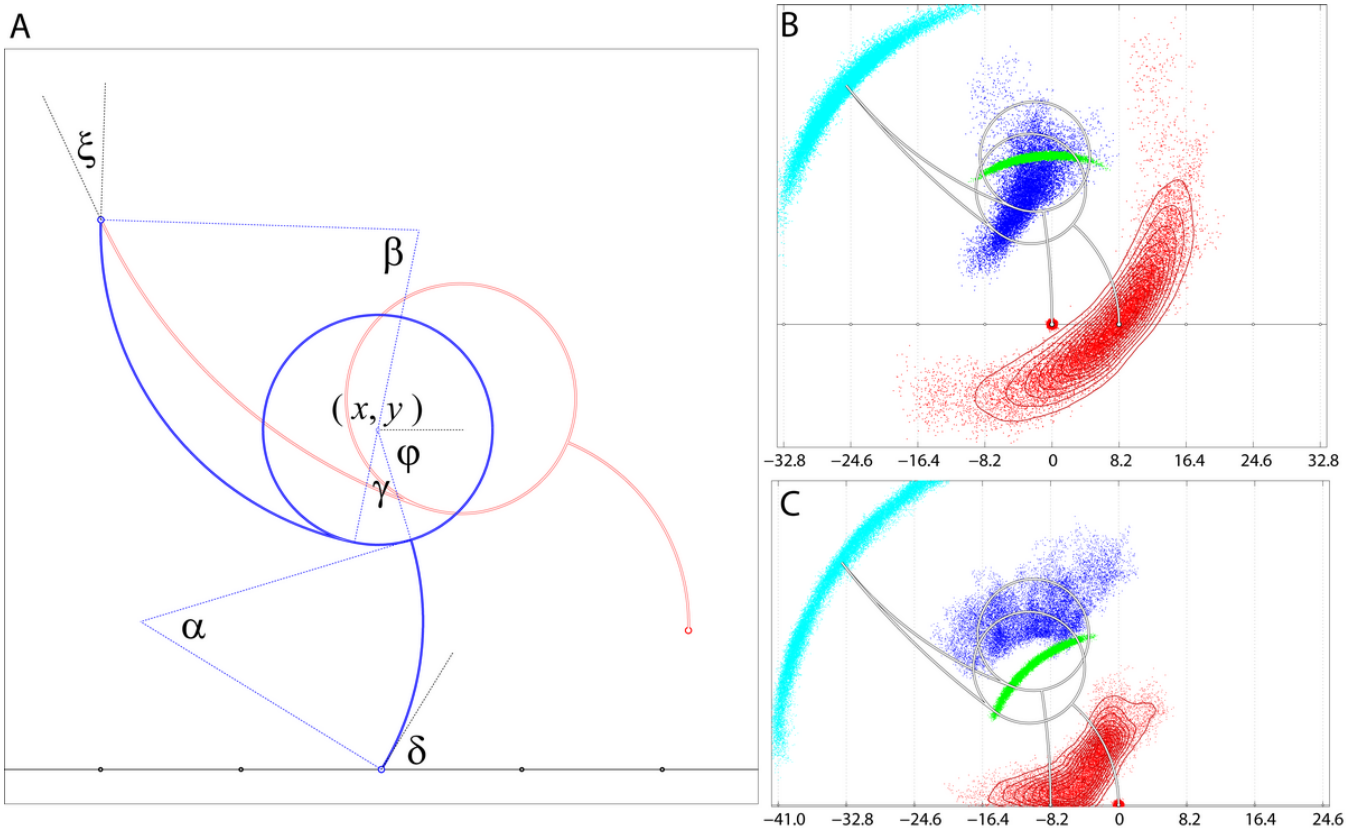
A
ξ
β
(x, y)
φ
γ
α
δ
B
−32.8
−24.6
−16.4
−8.2
0
8.2
16.4
24.6
32.8
C
−41.0
−32.8
−24.6
−16.4
−8.2
0
8.2
16.4
24.6

Figure S2

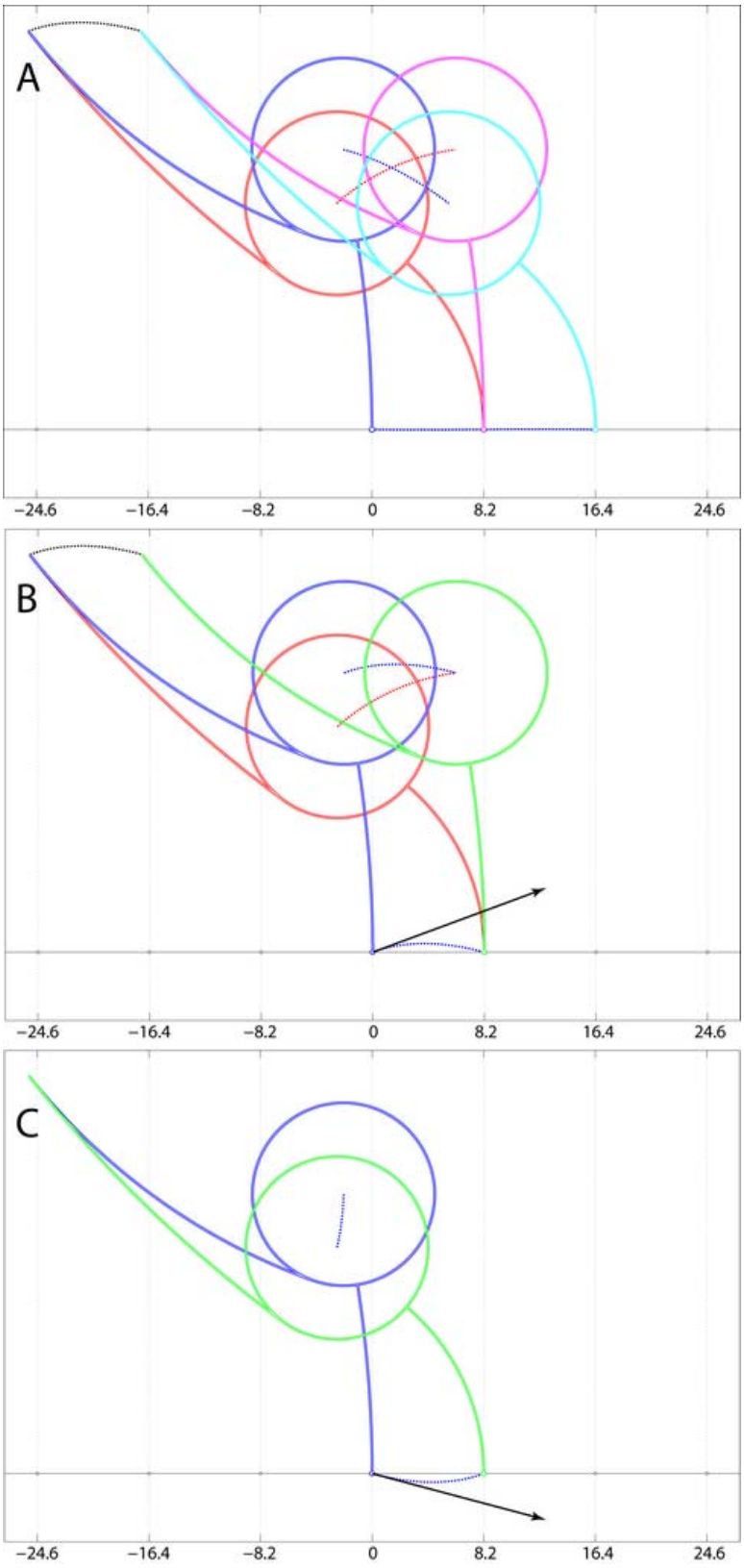
A
−24.6
−16.4
−8.2
0
8.2
16.4
24.6
B
−24.6
−16.4
−8.2
0
8.2
16.4
24.6
C
−24.6
−16.4
−8.2
0
8.2
16.4
24.6

Figure S3

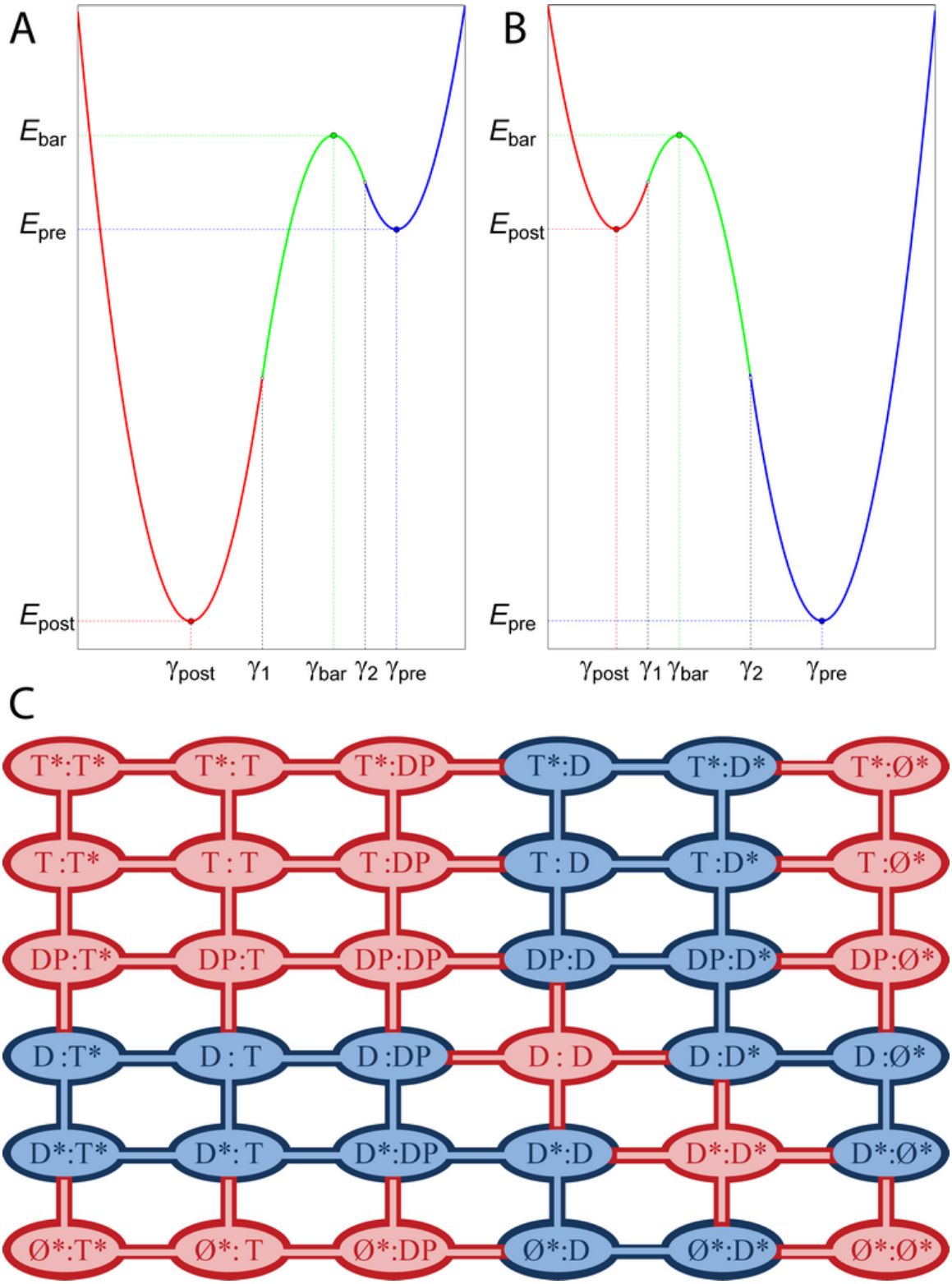
A
E_{bar}
E_{pre}
E_{post}
γ_{post} γ_1 γ_{bar} γ_2 γ_{pre}
B
E_{bar}
E_{post}
E_{pre}
γ_{post} γ_1 γ_{bar} γ_2 γ_{pre}
C
T*:T* T*: T T*:DP T*:D T*:D* T*:Ø*
T :T* T : T T :DP T : D T :D* T :Ø*
DP:T* DP:T DP:DP DP:D DP:D* DP:Ø*
D :T* D : T D :DP D : D D :D* D :Ø*
D*:T* D*: T D*:DP D*:D D*:D* D*:Ø*
Ø*:T* Ø*: T Ø*:DP Ø*:D Ø*:D* Ø*:Ø*

Figure S4